Strain-Induced Effects on Band-to-Band Tunneling and Trap-Assisted Tunneling in Si Examined by Experiment and Theory

Felipe Murphy-Armando,* Chang Liu, Yi Zhao, and Ray Duffy

Strain is commonly used in metal–oxide–semiconductor technologies to boost on-state performance. This booster has been in production for at least a decade. Despite this, a systematic study of the impact of strain on off-state leakage current has been lacking. Herein, experimental data and ab initio calculations are used to refine existing models to account for the impact of strain on band-to-band tunneling and trap-assisted tunneling in silicon. It is observed that the strain may dramatically increase the leakage current, depending on the type of tunneling involved. For band-to-band and trap-assisted tunneling, low uniaxial strains of 0.1% (or 180 MPa) can increase the leakage current by 60% and 10% compared to the unstrained case, respectively. Using models, it is predicted that compressive strain on the order of 1% (or 2 GPa) can increase the leakage current by 150 times. Conversely, tensile strain may diminish or at most double the leakage current in all observed cases. Though detrimental in conventional inversion-mode metal-oxide-semiconductor field-effect-transistor, these processes may be used to boost the performance of tunnel field-effect transistors, where on-state current is defined by band-to-band tunneling.

1. Introduction

Leakage currents in metal–oxide–semiconductor (MOS) devices are undesirable as they drain power supply resources in integrated circuits and systems. The International Roadmap for Devices and Systems[1] specifies leakage targets for current and future generation MOS technologies, but it is not fully understood how difficult many of these targets will be to achieve, which physical mechanisms are most responsible, and what should be done to alleviate the expected problems. Literature on diode leakage has been available for many decades; however, there are a number of aspects of modern MOS device processing and design that necessitates an update on the study of reverse-biased junction leakage. Strain is considered mandatory for modern and future CMOS technologies, for on-state performance enhancement.[2,3] This is achieved by an improvement of carrier mobilities in the device channel. Tensile strain is preferred for n-channel Si devices for electron mobility improvement, while compressive strain is better for p-channel Si devices. Strain can be introduced globally across the wafer, via epitaxial engineering of the substrate. Alternatively there are a number of local strain technologies including capping layers, such as SiN, or heteroepitaxial integration in the source and drain regions, such as SiGe in p-channel Si devices. However all these strain enhancements have focused on the on-state drive current in the MOS device, while relatively little study has been given to the impact of strain on the off-state. Off-state leakage current can originate at the reverse biased drain junction. Physical mechanisms to note here are band-to-band tunneling (BBT), Shockley–Read–Hall (SRH), and trap-assisted tunneling (TAT).

In this work we measure the leakage current as a function of strain in several Si diode samples, selected to isolate the contribution from the different tunneling mechanisms. We also wish to understand the leakage current under strain using available theory. It is our intention to use as few fitting parameters as possible. To accomplish this, we modify semiclassical, but still very relevant,[4] models of the BBT, SRH, and TAT currents in combination with ab initio electronic structure theory calculations. The latter are used to extract the electron–phonon coupling responsible for BBT and the strain effects on the band structure (effective masses, bandgaps, etc.) and carrier populations. The determination from first principles of SRH and TAT[5] and the dependence of defect states with strain[6] is still a very recent effort. Therefore, in this work we extract a best estimate of the

F. Murphy-Armando, R. Duffy
Tyndall National Institute, University College Cork
Lee Maltings
Dyke Parade, T12R5CP Cork, Ireland
E-mail: philip.murphy@tyndall.ie

C. Liu
School of Electronic Science and Engineering
Nanjing University
22 Hankou Rd, Nanjing 210093, China

Y. Zhao
Department of Information Science and Electronic Engineering
Zhejiang University
38 Zheda Rd, Hangzhou 310027, China

The ORCID identification number(s) for the author(s) of this article can be found under https://doi.org/10.1002/pssr.202400221.

ADVANCED
SCIENCE NEWS
www.advancedsciencenews.com

physica
pss status solidi rrl
www.pss-rapid.com

trap lifetimes and energies and their response to strain using the measured leakage currents and the calculated ab initio model of BBT. The trap energies and lifetimes are the only fitting parameters in our model, besides those related to avalanche breakdown.

We find that at stresses of up to 180 GPa the leakage current can be increased or reduced by the order of 5–10% and sometimes more at low voltages. Beyond the linear regime we predict that compressive strain can have a dramatic deleterious effect on the leakage current, leading to a 4–150 times increase for 1% uniaxial strain (≈2 GPa), due to large increases in the BBT current. Interestingly, BBT is the mechanism that makes tunnel field-effect transistors (TFETs) possible.[7] While an increase in BBT current is harmful to conventional mode metal-oxide-semiconductor field-effect-transistor, it can enhance the performance of TFETs, and strain is already being explored to this effect.[8]

2. Experimental Section

In a previous work,[9,10] Si diodes were fabricated carefully with different doping concentrations in the substrate in order to isolate different leakage mechanisms, including BBT, SRH, and TAT. This enabled a closer evaluation of these reverse leakage mechanisms. In summary, the process flow consisted of standard processing to define the active area and poly-buffered LOCOS isolation. A 5 nm screen oxide was deposited before the implants and anneals. For the n$^+$/p diodes, high-concentration arsenic was implanted shallow and then given a high thermal budget anneal of 1100 °C for 5 min to drive in the dopant. Thereafter the low-concentration doped region was formed by a boron implant. The sample notation refers to this process: AB for arsenic–boron samples, and BA for boron–arsenic samples (the BA samples are not used in this work). The rest of the flow consisted of an 1100 °C 0 s spike anneal to activate the dopants, a clean step to remove the screen oxide, and the deposition of a Ti/TiN contact layer. Finally a 650 nm layer of AlCu metal was deposited and patterned. See inset in Figure 4 for a schematic of the diode structure.

Current–voltage characteristics of the fabricated diodes were measured using a HP4155 parameter analyzer. A thermochuck was used to investigate temperature dependency. For each structure and split several die were measured. Most of the measurements were done on square diodes, consisting of a rectangular active area with a high $\frac{\text{area}}{\text{perimeter}}$ ratio. For completeness perimeter current was extracted by comparing currents from meander structures with the same area but different isolation perimeters, and this was subtracted from the total square diode current. In all square diodes, the perimeter component of the leakage current was several orders of magnitude lower than the area contribution. For details on the temperature dependence of the leakage current and the doping profile of the diodes, we refer the reader to refs. [9,10]. The mechanical stresses were applied using a four-point wafer bending system. Using this system, we studied the effects of both uniaxial tensile and compressive strain. Details of the mechanical stress equipment can be found in refs. [11,12].

3. Refined Model Accounting for Strain

To account for the effects of strain on the leakage current, we modify the established models by Schenk[13] for BBT and Hurkx for SRH and TAT.[14] The band structure of Si under strain is calculated using the 30-band k.p model of Rideau et al.[15] The electron–phonon coupling necessary for the BBT is calculated using density functional perturbation Theory, available in the code Abinit,[16,17] as in refs. [18–20]. The total current density may be modeled by[14]

$$j_d = \frac{\left(j_{bbt}\phi(0) + e\int_{-x_p}^{x_n} R_{trap}(x)\phi(x)dx\right) + j_i(1 + \phi(x_n))/2}{1 - \int_{-x_p}^{x_n} \alpha_n(x)\phi(x)dx} \tag{1}$$

where $\phi(x)$ is defined in ref. [14] as

$$\phi(x) = e^{-\frac{1}{2}\int_{-x_p}^{x_n} \alpha_n(x')dx'} \tag{2}$$

with the ionization coefficient

$$\alpha_n(x) = \alpha_{n\infty} e^{-\frac{b_n}{|F(x)|}} \tag{3}$$

where $F(x)$ is the electric field and $\alpha_{n\infty}$ and b_n are fitting parameters related to avalanche breakdown.

The ideal diode current density j_i is given by

$$j_i = j_s\left(e^{eV/kT} - 1\right) \tag{4}$$

where $j_s = en_i^2\left(1/N_a\sqrt{D_n/\tau_n} + 1/N_a\sqrt{D_p/\tau_p}\right)$ is the saturation current density, assuming a step doping profile, and e is the electron charge, $n_i = \int dE f(E)g(E)$ is the intrinsic carrier concentration with $f(E)$ and $g(E)$ the Fermi distribution and density of states (DOS), respectively, determined by the calculated electronic band structure. N_a and N_d are the acceptor and donor densities, D_n and D_p the diffusion charge coefficients, and τ_n and τ_p are the electron and hole lifetimes. At the carrier concentrations considered in this work, the contribution of j_i to the total current is negligible.

The TAT rate R_{trap} including the Poole–Frenkel effect is given by Equation (6) of ref. [21].

$$R_{trap}(x) = \frac{n(x)p(x) - n_i^2}{\tau\left[\frac{n(x) + n_i e^{(\overline{E}(x))/kT}}{1 + \Gamma_p(x)} + \frac{p(x) + n_i e^{(-\overline{E}(x))/kT}}{1 + \Gamma_n(x)}\right]} \tag{5}$$

where $\overline{E}(x) = E_T - E_i(x)$, E_T and E_i are the average trap and intrinsic Fermi energies, respectively. R_{trap} becomes the SRH tunneling rate when the field-effect function[21] $\Gamma \ll 1$ is at low electric field.

In contrast to ref. [21], we consider the six conduction and three valence band valleys independently. Therefore we redefine the field-effect functions

$$\Gamma_n = \sum_c r_c \Gamma'_{n,c} \tag{6}$$

$$\Gamma_p = \sum_v r_v \Gamma'_{p,v} \tag{7}$$

where the sums are over the conduction bands at the six valleys at the Δ points in the Brillouin zone, 83% along the Γ–X line (index $c = \Delta_{\pm x}, \Delta_{\pm y}, \Delta_{\pm z}$) and three valence bands, heavy holes (HH), light holes (LH), and split-off band (SO) (index $\nu = $ HH, LH, SO), $r_j = n_j/n_T$, are the fractional occupation of each band j, with $n_j = \int dE f_j(E) g_j(E)$ and $n_T = \sum_j n_j$. The field-effect functions $\Gamma'_{n,c}$ and $\Gamma'_{p,v}$ are as defined in Equation (7) of ref. [21], but for each band

$$\Gamma'_{n,c} = \frac{\Delta E_{n,c}}{kT} \int_0^1 \exp\left(\frac{\Delta E_{n,c}}{kT} u - K_{n,c} u^{3/2}\right) du \tag{8}$$

$$K_{n,c} = \frac{4}{3} \frac{\sqrt{2 m_{n,c}^{\parallel} \Delta E_{n,c}^3}}{e\hbar|F|} \tag{9}$$

and analogously for $\Gamma'_{p,v}$. The effective mass $m_{n,c}^{\parallel}$ corresponds to that in the transport direction for an electron in conduction band c, $\Delta E_{n,c}$ and $\Delta E_{p,\nu}$ are given by Equation (9a) and (9b) of ref. [21].

$$\Delta E_{n,c} = \begin{cases} E_c(x) - E_{cn}, & E_T(x) \leq E_{cn} \\ E_c(x) - E_T(x), & E_T(x) > E_{cn} \end{cases} \tag{10}$$

and

$$\Delta E_{p,v} = \begin{cases} E_{vp} - E_v(x), & E_T(x) > E_{vp} \\ E_T(x) - E_v(x), & E_T(x) \leq E_{vp} \end{cases} \tag{11}$$

$E_{c(v)}(x) = E_{c0(v0)} - \psi(x)$ is the local conduction band minimum (valence band maximum) and is given by the band structure at zero field and the local electrostatic potential, $\psi(x)$, defined below. $E_{cn} = E_c(x_n)$ and $E_{\nu p} = E_\nu(-x_p)$ are the conduction and valence band edges at the n and p sides, respectively. $x_{n,p}$ are the positions of the n and p sides, defined below.

The coefficients r_ν and r_c are new to the model, give the proportional occupation of each of the valence (ν) and conduction (c) bands, and depend on the amount of strain (see **Figure 1**a,d for the strain dependence of r_c and r_ν). All parameters have been calculated as strain dependent.

To calculate the BBT current in an indirect semiconductor, we use as a basis the model derived by Schenk,[13] given by

$$j_{bbt} = \frac{12\pi e^2}{\hbar^5} \sum_{i,c,v} r_c r_v$$

$$\times \left(|V_{c,i}^e|^2 \left|\frac{p_{c,v}(\Gamma)}{E_{c,v}^{dg}(\Gamma)}\right|^2 + |V_{v,i}^p|^2 \left|\frac{p_{c,v}(\Delta)}{E_{c,v}^{dg}(\Delta)}\right|^2 \right)$$

$$\times \frac{\sqrt{m_t^2 m_l}\, m_{DOS,v}^{3/2}}{m_e^2} F_m \left[\left(E_{c,v}^{ig} - \hbar\omega_i\right) N_i H\left(x_{i,c,v}^-\right) \right.$$

$$+ \left(E_{c,v}^{ig} + \hbar\omega_i\right)(N_i + 1) H\left(x_{i,c,v}^+\right) \Big]$$

$$\times \left(f_v(\Gamma) - f_c(\Delta)\right) \tag{12}$$

$$H(x) = \frac{Ai(x)}{x^2} + \frac{Ai'(x)}{x} + Ai_1(x) \tag{13}$$

$$x_{i,c,v}^{\pm} = 2^{2/3}\left(E_{c,v}^{ig} \pm \hbar\omega_i\right)\left(\frac{2\mu_{c,v}}{e^2 \hbar^2 F_m^2}\right)^{1/3} \tag{14}$$
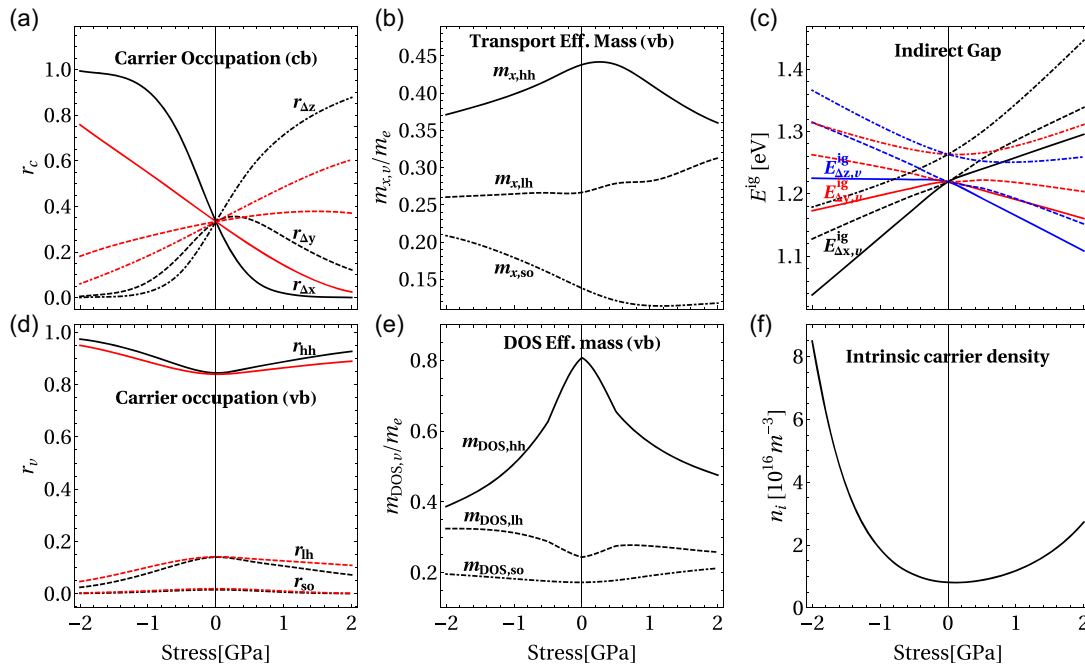

Figure 1. Theoretical a) relative occupation of the conduction and d) valence band valleys versus. strain for doping densities 1.9×10^{18} cm^{-3} (black) and 2.15×10^{20} cm^{-3} (red). The labels Δx, y, and z refer to the Δ valleys along the three Cartesian axes. The labels hh, lh, and so refer to the heavy hole, light hole, and split-off valence bands of Si, respectively. b) Conductivity mass versus stress of the topmost valence bands in the x direction. c) Intrinsic energy gap versus stress between the conduction band valleys (x, y, and z valleys at Δ represented by black, red, and blue, respectively) and the topmost valence bands (top: solid, second top: dashed, SO band: dot-dashed). e) DOS mass versus strain of the three topmost valence bands. f) Intrinsic carrier concentration versus stress.

ADVANCED
SCIENCE NEWS

www.advancedsciencenews.com

physica pssrrl
status
solidi

www.pss-rapid.com

where $Ai(x)$, $Ai'(x)$, and $Ai_1(x)$ are Airy functions, $\pm$ corresponds to emission (+) and absorption (−) of a phonon, $V_{c,i}^e$ and $V_{v,i}^p$ are the electron- and hole-phonon scattering potentials between states at Γ and Δ, at the conduction and valence band, respectively, and $p_{c,\nu}(\Gamma \text{ or } \Delta)$ are the optical valence-conduction coupling constants at Γ and Δ. The terms involving $V_{c,i}^{e/p}$ and $p_{c,\nu}(\Gamma \text{ or } \Delta)$ involve the two processes shown in **Figure 2** between the valence and conduction bands via the dipole and electron–phonon matrix elements. It is analogous to the process of indirect photon absorption, where the electric field coupling is given by that of the photon, rather than the field across the junction.

The masses m_t, m_l, and $m_{\text{Dos},\nu}$ correspond to the transverse and longitudinal masses at the conduction band at Δ and the DOS mass of the valence band at Γ. $E_{c,\nu}^{\text{ig(dg)}}$ is the indirect (direct) bandgap between the conduction band c and valence band ν (see Figure 2), ω_i is the frequency of phonon mode i involved in the transition, N_t is the number of phonons in mode i, given by the Bose–Einstein distribution, and $f_n(m)$ is the electronic distribution of band n at the m k-point (Γ or Δ). The reduced mass $\mu_{c,\nu}$ is given by the conductivity masses in the direction of the current

$$\frac{1}{\mu_{c,\nu}} = \frac{1}{m_v^\parallel} + \frac{1}{m_c^\parallel} \tag{15}$$

where $m_c^\parallel$ depends on the conduction band valley and is given by $m_{cx}^\parallel = m_{cy}^\parallel = 0.19 m_e$ and $m_{cz}^\parallel = 0.95 m_e$, and $m_v^\parallel$ is given below in Equation (22) and (23).

The maximum electric field F_m and the depletion width W in terms of the applied voltage were calculated using the Poisson equation. Our model can take as input the measured doing profiles, if necessary. In our calculations we wished to ascertain how far the calculations depend on idealized conditions or actually measured quantities. Therefore we consider two sources for the doping profiles: those measured as a function of diode

coordinate in refs. [9,10], and an ideal version calculated from a step doping profile, given below. Due to the simplicity of the measured doping profile, we found no significant difference from either profile in all the results of current versus strain and voltage in this article. The step doping profile is given by the potential

$$\psi(x) = \begin{cases} \frac{eN_a}{2k_0}(x + x_p)^2, & x < -x_p \\ V_d - V - \frac{eN_d}{2k_0}(x - x_n)^2, & -x_p \le x \le x_n \\ V_d - V, & x > x_n \end{cases} \tag{16}$$

with k_0 the dielectric permittivity, that results in an electric field

$$F(x) = \begin{cases} F_m\left(1 - \frac{|x|}{x_p}\right), & x < 0 \\ F_m\left(1 - \frac{|x|}{x_n}\right), & x \ge 0 \end{cases} \tag{17}$$

where the coordinates for the pure n and p sides are given by

$$x_{n,p} = \sqrt{\frac{2N_{a,d}k_0 V_d(1 - V/V_d)}{eN_{d,a}(N_d + N_a)}} \tag{18}$$

The maximum electric field is

$$F_m = 2\frac{V_d}{W}\left(1 - \frac{V}{V_d}\right)^{\frac{1}{2}} \tag{19}$$

with the junction width given by

$$W = \sqrt{(2k_0/e)\left(\frac{1}{N_d} + \frac{1}{N_a}\right)(V_d - V)} \tag{20}$$

and the junction voltage V_d given by

$$V_d = E_{Fn} - E_{Fp} \tag{21}$$

where E_{Fn} and E_{Fp} are the quasi Fermi energies in the n and p sides respectively. The DOS and conductivity masses at the valence band are parametrized from the total band structure as an average in the occupation of holes[22]

$$m_{\text{DOS},v}^{3/2} = \frac{\pi^2 \hbar^3}{\sqrt{2}(kT)^{3/2}} \frac{n_v}{\int \frac{\sqrt{x}}{1 + e^{x - (E_v - E_F)/kT}} dx} \tag{22}$$

and

$$m_v^\parallel = \left(\int \frac{1}{m_v(k)}(1 - f_v(k))dk\right)^{-1} \tag{23}$$

respectively, with E_ν the energy of valence band ν, and E_F the Fermi level. See Figure 1b,e for the stress dependence of the current and DOS masses, respectively.

All parameters in the BBT current density are determined ab initio. The intervalley electron–phonon coupling is given by the intervalley deformation potentials as

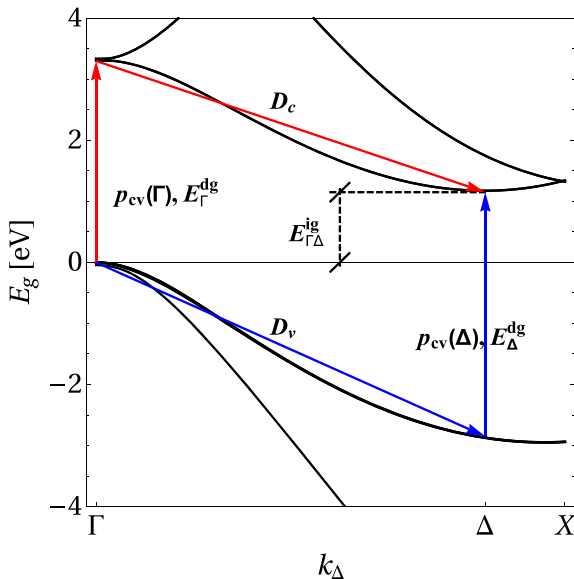$$\left|V_{c/v,i}^{e/p}\right|^2 = D_{c/v}^2 \frac{\hbar}{2\rho\omega_i} \tag{24}$$

Figure 2. Theoretical electron–phonon channels considered in BBT, shown on the electronic band structure of Si.

ADVANCED SCIENCE NEWS
www.advancedsciencenews.com

pss rrl
physica status solidi
www.pss-rapid.com

where $D_{c/v}$ is the intervalley deformation potential for a phonon linking the Γ and Δ at the conduction/valence band, ρ is the atomic density, and ω_i is the frequency of phonon with polarization i. The calculated deformation potentials and frequencies are listed in Table 2. The dipole matrix elements between valence and conduction band are determined from the k.p model Hamiltonian H_k as $p_{c,v} = \langle \phi_c | \nabla_k H_k | \phi_v \rangle$. The dipole matrix elements and direct bandgaps versus stress at the Γ k-point are shown in **Figure 3**a,b, respectively. The dipole matrix elements at the Δ k-point are stress independent with values for $|p_{\Delta c,v1}| = |p_{\Delta c,v2}| = 0.57$ and $|p_{\Delta c,so}| = 0$, in atomic units. The direct bandgaps versus stress at the Δ k-point are shown in Figure 3c.

4. Fitted Quantities

In Equation (12), the only free parameter affecting the BBT current is the doping concentration. Therefore, we determine the effective densities of acceptor impurities N_a for samples AB1 and AB3 at zero strain by the BBT-dominated current at high $|V|$. In AB5 we determine N_a together with the trap lifetime τ and trap energy E_T. The effective impurity densities N_a for all samples are shown in **Table 1**. All agree within a factor of 2 with the maximum experimentally determined doping densities at the junctions[9] of 6.1×10^{18}, 1.9×10^{18}, and 1×10^{17} for AB1, AB3, and AB5 respectively. **Figure 4** shows the measured and modeled current densities at zero strain for the samples considered. The

Table 1. Fitted parameters used in Equation (1) and (3). The values in parentheses are the experimentally determined maximum doping densities at the junction from ref. [9].

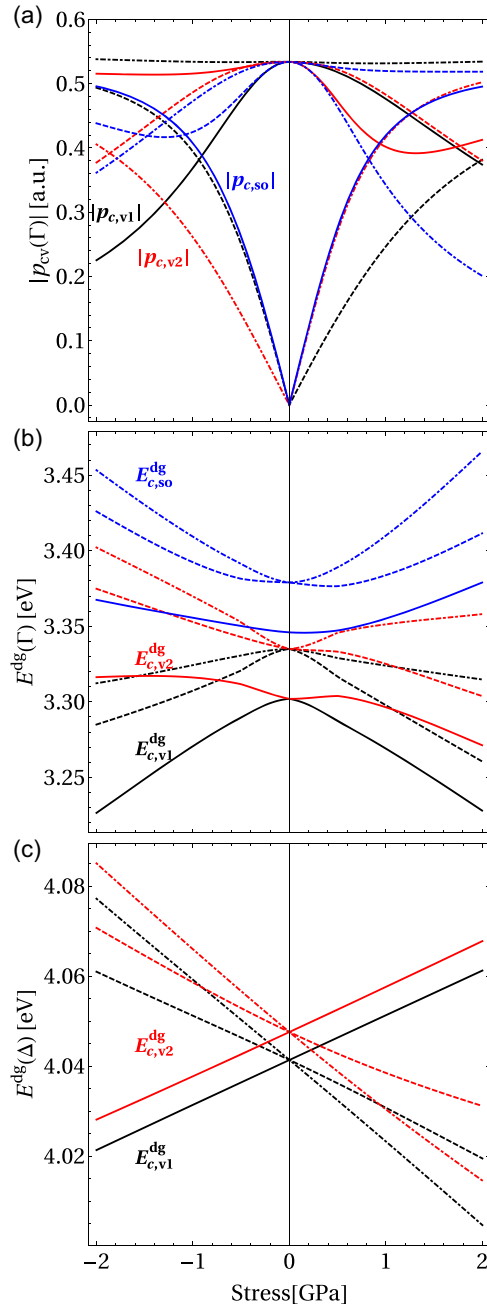|	AB1	AB3	AB5
N_a [10^{17} cm^{-3}]	35.63 (61)	14.82 (19)	2.5 (1)
$a_{n\infty}$ [m^{-1}]	1	1.824×107	6.9×10^{6}
b_n [V m^{-1}]	1	3.0×10^{5}	1

Figure 3. Theoretical a) dipole matrix element, b) direct bandgap at Γ, and c) direct bandgap at Δ versus stress between the first three conduction bands at Γ (with increasing energy represented by solid, dashed, and dot-dashed) and the three topmost valence bands (top: black, second top: red, SO split-off band: blue). The direct bandgap $E_{c,so}^{dg}(\Delta) \gg E_{c,(v1,v2)}^{dg}(\Delta)$, resulting in a negligible term in j_{bbt}, and is therefore not shown.
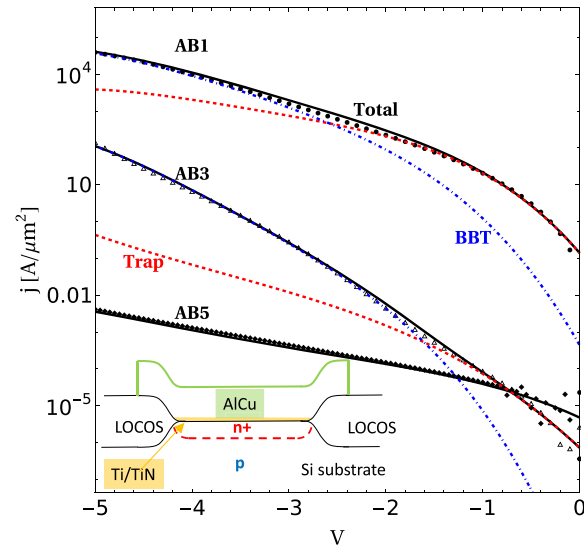

Figure 4. Experimental (points) and modeled (solid) current density versus reverse bias voltage for the three samples considered. The modeled current is composed of BAT (blue, dot-dashed), TAT (red, dashed), and total current (black solid). Inset: Schematic of the diode structure.

agreement between the model and the measurements is excellent, and the first-principles part of the model that depends on the band structure and electron–phonon transitions is validated.

Many of the parameters involved in TAT are very hard to calculate a priori, as the number, energy and lifetimes of the traps depend on the sample growth conditions. We have therefore fitted the lifetime τ and the trap energies E_T to our experiments.

Measurement of trap energies and lifetimes in Si exists in the literature,[23] but is of course spread in a range of values. Our fitted values are consistent with earlier measurements. Furthermore, to our knowledge, this is the first publication that considers the effect of strain on trap energies and lifetimes. From Equation (5) we can see that τ is a scaling factor at all voltages. The effect of E_T is more complicated, in that it changes the slope of the current versus voltage. Therefore, E_T has a large effect on
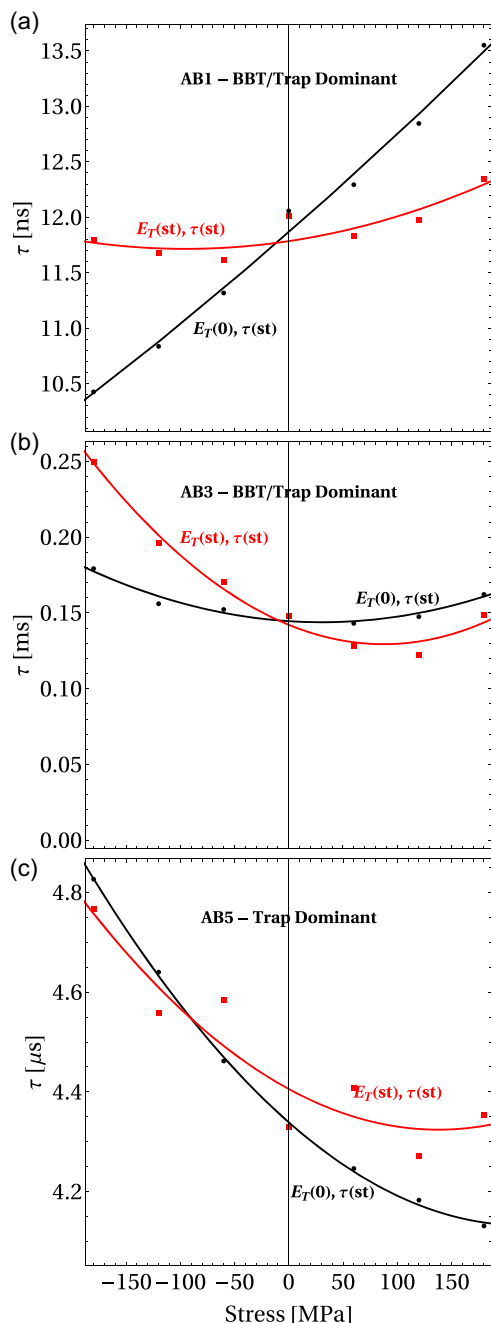

Figure 5. Fit trap lifetime τ versus strain for samples a) AB1, b) AB3, and c) AB5. The fit values depend on whether the trap energy E_T is strain dependent (red) or not (black). The currents corresponding to these values are shown in Figure 9 and 10.
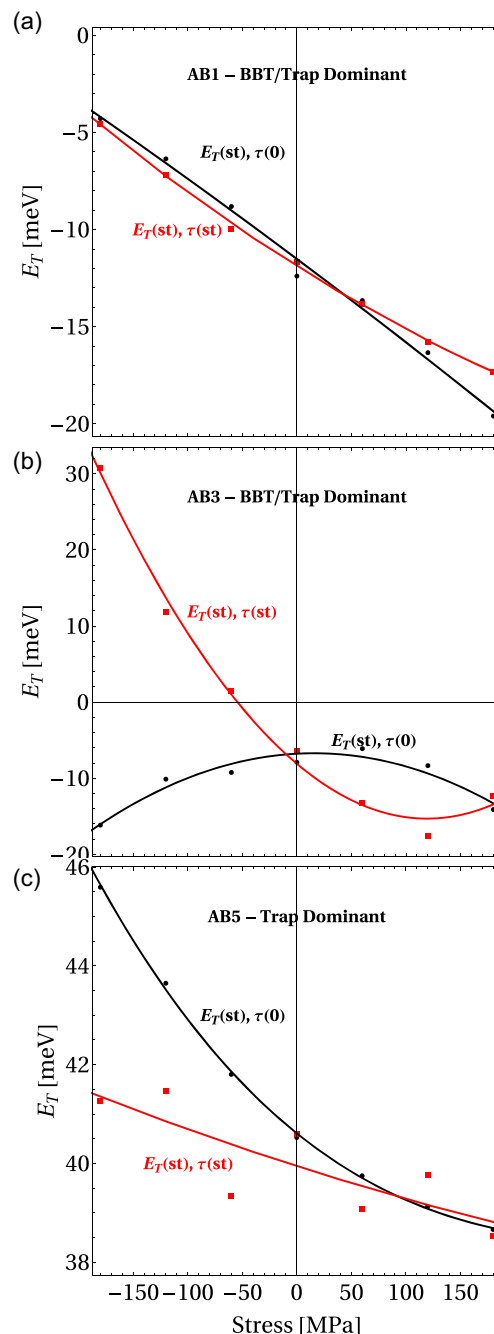
Figure 6. Fit trap energies E_T versus strain for samples a) AB1, b) AB3, and c) AB5. The fit values depend on whether the trap lifetimes τ are strain dependent (red) or not (black). The currents corresponding to these values are shown in Figure 9 and 10.

Table 2. Calculated electron–phonon deformation potentials and phonon energies for the phonons involved in BBT.

Phonon	$\hbar\omega$ [meV]	D_c [eV Å^{-1}]	D_ν [eV Å^{-1}]
2TA	17	0.15	0.28
LA	42	4.6	4.9
LO	57	0	7.2
TO	57	5.4	2.7

the response to strain, affecting the sign of the slope of the current versus strain.

We considered trap lifetime τ and trap energy E_T to be strain dependent and voltage independent. The best fit to the measured current versus stress is given by a cubic dependence on stress. The resulting fits for τ and E_T versus stress are shown in **Figure 5** and **6**, respectively.

The values for τ and E_T are meant to reflect the effective values for an undetermined, sample-dependent variety of trap states. We believe that the cubic dependence at higher stresses is unlikely and rather expect a saturation or at least a linear behavior. We therefore consider three further limiting cases for the stress effect on the trap-assisted current: both or either τ and E_T constant with stress. The resulting values considering these cases for the fitted τ and E_T with stress are shown in Figure 5 and 6.

The electron–phonon process responsible for BBT is related to that causing indirect photon absorption and emission in Si. This has been explored from first principles in a previous work.[24]
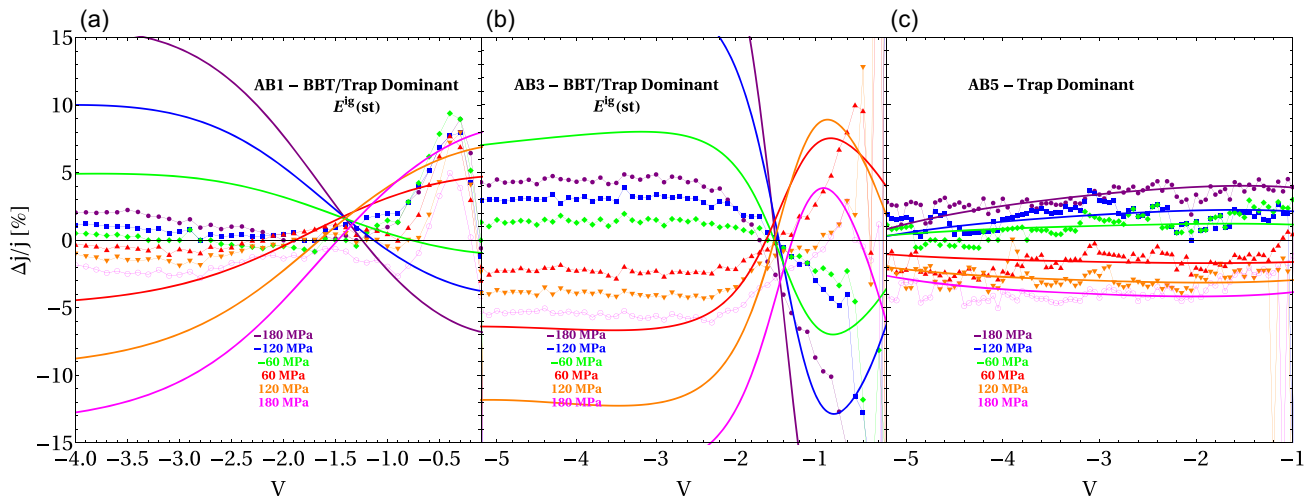

Figure 7. Experimental (joined points) and modeled (solid) current density change (in percent) versus reverse bias voltage for samples a) AB1, b) AB3, and c) AB5 at six different stresses (−180, −120, −60, 60, 120, 180) MPa represented as purple, blue, green, red, orange, and magenta.
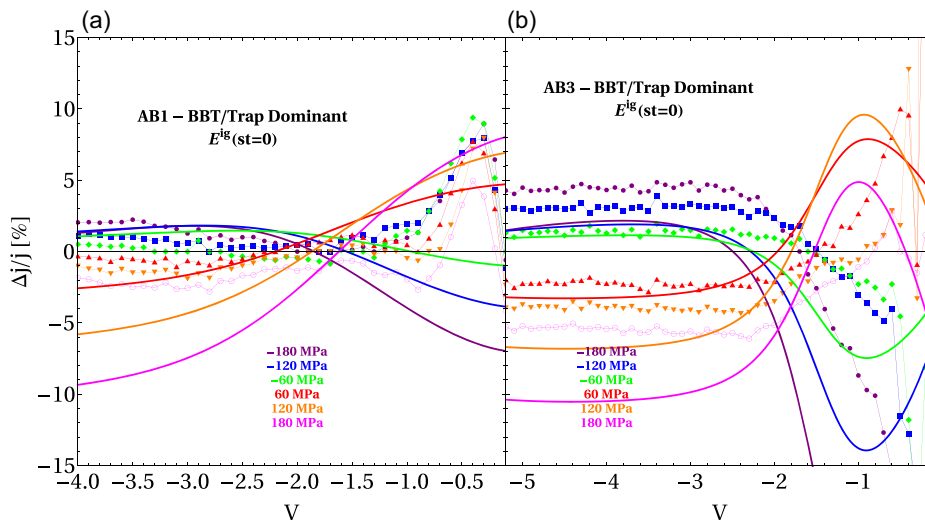

Figure 8. Experimental (joined points) and modeled (solid) current density change (in percent) versus reverse bias voltage neglecting the strain dependence of E^{ig} for samples a) AB1 and b) AB3, at six different stresses (−180, −120, −60, 60, 120, 180) MPa represented as (purple, blue, green, red, orange, and magenta).

However the deformation potentials have not been published, and hence we present ours here in **Table 2**. Vandenberghe and Fischetti[25] have also studied BBT via ab initio calculations of the electron–phonon coupling parameters. However, they considered a direct valence-to-conduction electron–phonon route, rather than one mediated by the electric field, as in the analysis by Schenk[13] (see Figure 2). The direct valence-to-conduction electron–phonon route would only be valid for overlapping valence and conduction band energies to within the phonon energy. The coupling resulting from the latter channel would be independent of the electric field, except indirectly through the change in the valence and conduction band energies. We believe this channel would have a very small contribution at the electric fields considered in this work and is therefore neglected. We present the calculation of the current densities with parameters calculated entirely ab initio and find good agreement to our measured currents in BBT-dominant samples at zero strain (see Figure 4). This is important, as it indicates that as far as BBT is concerned, the material behaves like ideal doped silicon and that the model captures most of the physics involved.

5. Discussion

We measured and calculated the reverse bias current percent change along the (001) direction as a function of uniaxial stress in the (100) direction in all the samples. **Figure 7** shows these for samples AB1, AB3, and AB5, respectively. For such small stresses, the change in current density affected by the strain is quite large, up to several percent for strains of up to 0.13% (see also results for the p-type case of sample BA2 in ref. [26]). At voltages $-0.5 < V < 0$, the measured change of the current with stress can be of several 10 s of percent (not shown). From Equation (5) and (12), we expect the behavior of TAT and BBT currents to be very different under applied strain. From our model, samples AB1 and AB3 are dominated by TAT between 0 and -1.5 V, and BBT thereafter (see Figure 4). The response to strain of the crossover from TAT to BBT at -1.5 V can also be clearly seen in Figure 7.

Our model reproduces the current versus voltage behavior very well, but overestimates the response to strain compared to the measurements in this work. Since the BBT model is entirely based on first principles, we expect the calculated larger calculated response to strain to be valid in the ideal case and that nonideal effects on the samples may be at play. There may be several reasons for these, such as reduced transfer of stress into the sample, or the effect of very high doping on the strain response of the bandgaps. In our calculations, we did not include any effects of the doping on the bandgaps and effective masses. The BBT is exponentially sensitive to variations in the indirect bandgap, and doping may reduce its change with strain. This effect is clearly seen in **Figure 8**, which shows the effects of neglecting the strain dependence of the indirect bandgap E^{ig} on the current response to stress in Equation (12). A stress-independent E^{ig} while keeping all other stress dependencies, produces excellent agreement to experiment. This suggests that the overlap of the decaying electron and hole wavefunctions at each side of the junction is not changing with stress as fast as in the model. We expect, however, the sensitivity of E^{ig} to strain

to increase at higher strains, as the higher-energy separation between valleys cannot be compensated by the doping charge. Measurements at higher strains and further study into the effects of doping on the bandgap in the presence of strain are required to answer these questions.
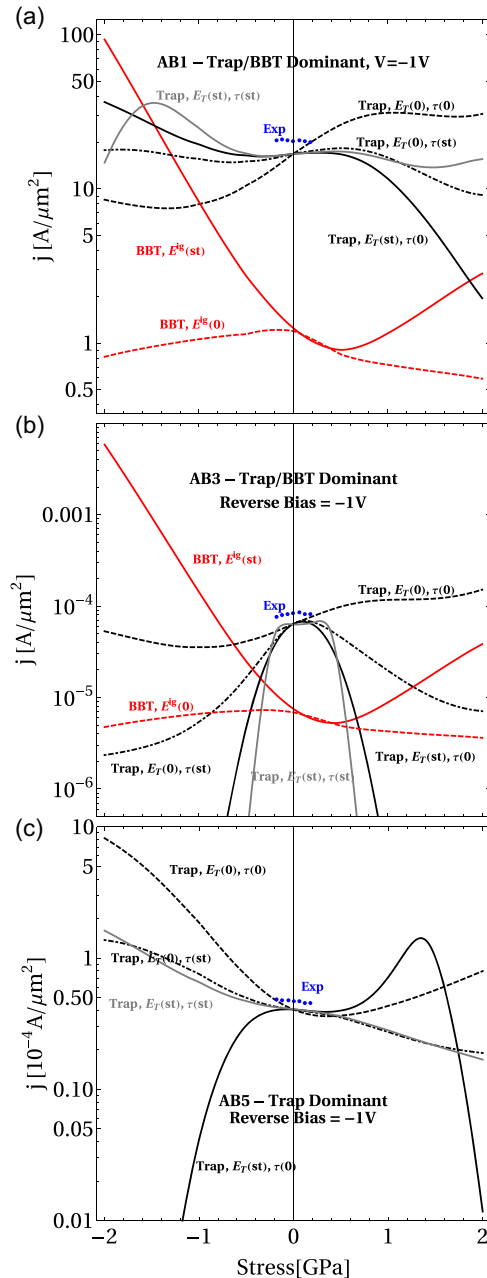

Figure 9. Contributions from the currents of samples a) AB1, b) AB3, and c) AB5 due to BBT (red) and trap (black and grey) versus applied stress at a reverse bias voltage of -1 V. The current represented by the dashed BBT curve neglects the strain contribution to the indirect gap E^{ig}. The solid BBT curve includes the full strain dependence. The trap-assisted currents are calculated with full strain dependence of E_T and τ (grey), only E_T (solid), only τ (dot-dashed), and strain-independent E_T and τ (dashed) (see Figure 5 and 6 for the strain dependence of τ and E_T). The blue points correspond to the experimentally measured current density.
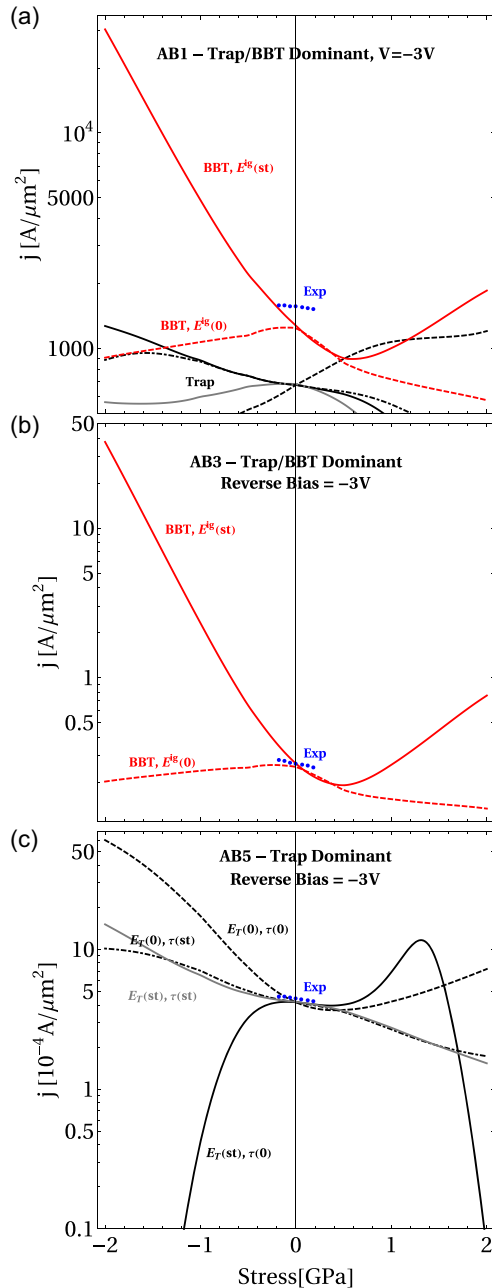
2400221 (8 of 11)

Figure 10. Contributions from the currents of samples a) AB1, b) AB3 and c) AB5 due to BBT (red) and Trap (black) versus applied stress at a reverse bias voltage of −3 V. The current represented by the dashed BBT curve neglects the strain contribution to the indirect gap E^{ig} and to the effective mass in the transport direction. The solid BBT curve includes the full strain dependence. The Trap assisted currents are calculated with full strain dependence of E_T and τ (grey), only E_T (solid), only τ (dot-dashed) and strain independent E_T and τ (dashed) (see Figure 5 and 6 for the strain dependence of τ and E_T). The blue points correspond to the experimentally measured current density.

shown in **Figure 9** and **10** at voltages of −1 and −3 V, respectively. Strain affects BBT and TAT differently, as shown in Figure 9. We get excellent agreement between theory and experiment for the current density at zero strain. However, at stresses up to 180 MPa, our theoretical model overestimates the response to strain compared to our experiment. This may be due to a variety of reasons, as explained earlier in the text. We find that the best quantitative agreement with experiment that retains the same linear behavior of current versus stress is given by neglecting the stress dependence of the indirect gap E^{ig} in Equation (12) (see Figure 8). However, as explained earlier, we don't expect E^{ig} to remain independent at stresses higher than 180 MPa. In our prediction of the BBT leakage current, we consider both limiting factors: 1) complete stress dependence of all parameters; and 2) stress independence of E^{ig}. These two cases are shown in Figure 9 for −1 V and 10 for −3 V as the red solid and dashed lines respectively. We observe that, except at small strains, the stress dependence of the current via the indirect gap is very strong. We must remark that the agreement of the model with experiments at low strains does not imply that stress dependence via E^{ig} is negligible at higher strains. This stress dependence is very strong and predicted in the first-principles model, and while it may be masked at lower strains by other factors, it should dominate at higher strains.

Notably, the full stress-dependent BBT is most sensitive to compressive stress. Under enough compressive stress, BBT can become dominant over the other tunneling mechanisms. Worryingly, the leakage current can increase by 4 to 80 times in TAT- and BBT-dominant devices under compressive stress at $V = −1$ V, and up to 20–150 times at higher voltages, where the current is dominated by BBT. Conversely, tensile stress affects the leakage to a lesser degree and may reduce it at low stresses in purely BBT transport.

At this stage, it is hard to predict the effect of high strain on TAT. However, we can study the range of possible values under different regimes of extrapolation of the two unknown variables E_T and τ. These cases are shown in Figure 9 and 10. We explore the cases in which there is stress dependence in: 1) neither E_T or τ (black dashed line); 2) only E_T (solid black); 3) only τ (black dot-dashed); and 4) both E_T and τ (gray). Since both E_T and τ are fit by a cubic function of stress (see Figure 6 and 5), this extrapolation to 2 GPa becomes very unrealistic. It may serve however as a limiting case. We expect the values of E_T and τ to saturate at some point. Considering this, case (1) might give a reasonable expectation of the TAT current density at high stress. In general, we can expect TAT-dominant leakage to increase less than 20 times under 2 GPa stress. We expect the case of strain-independent effective trap energies and lifetimes and strain-dependent lifetimes to be the closest to reality, for the following reasons. Generally, there are multiple trap states that have different energies and lifetimes. Our model simplifies the effect of all these traps into that of one, effective trap state. At high strains, the shift in the average energy of multiple trap states is likely to be less than an effective state, as states that move out of the tunneling window of energies are replaced by those entering it from the opposite extreme. The lifetimes are more likely to change if the stress environment is similar for all traps present.

Nowadays, strain of the order of 1% is commonly used to increase the mobility of transistor channels. We explore the effects of such strains ($\approx$2 GPa in Si) on the leakage current,

6. Conclusion

We combined experiment and theory to determine the effects of strain on the components of the tunneling current in silicon diodes in reverse bias. We focused on diodes at three specific doping concentrations in which the current is dominated by either BAT or TAT. The reverse bias current in the three diodes was measured at (100) uniaxial stress in the range of ±180 MPa. At the same time, we refined existing models of the band-to-band and TAT to account for the effects of strain. Whenever possible, we endeavored to keep the models free from experimental parameters. This was possible entirely in the modeling of BAT, where the electronic band structure and electron-phonon coupling parameters required for the calculation of the current have been calculated using first-principles electronic structure methods.

The parameter-free description of TAT is possible to a degree. The details of the band structure and its response to strain can be treated in this way. However, the responses to strain of the trap lifetimes and energies are not known. We attempted to gain an understanding of this response, albeit crude, by fitting effective trap energies and lifetimes to our measurements versus voltage and strain. The effective trap lifetimes and energies were the only fitting parameters in this otherwise parameter-free model.

The agreement between the model and experiment of the trap-assisted current is very good, in part due to the lifetimes and energies being fitted. The agreement is worse for the highly doped samples where other effects may take place at low voltages. The crossover from trap-assisted to BAT with increasing voltage is well captured by the model.

The agreement of the band-to-band component of the current with strain is less satisfactory. Our model predicts a response of the current with strain that is five times larger than the one measured. Having no parameters to fit, the model relies on the samples behaving as pure Si, and the strain being perfectly transferred across the sample. We found the only effect consistent with measurement to be the lack of a strain dependence of the bandgap. This may be due to the large doping concentration and small strains considered and warrants further study using higher strains and a model explicitly considering dopant states.

We used our theoretical model to venture a prediction of the tunneling current at higher uniaxial stresses of up to 2 GPa, as typically found in stress-enhanced transistor channels. We predict that strain can have a very large effect on the leakage current, especially in band-to-band-dominated samples. At low voltages, compressive strain can switch trap-assisted tunneling to a band-to-band-dominated current. If, however, the strain dependence of the bandgap is small or absent as suggested by the measurements at small strain, BAT may be largely insensitive to strain.

We find that trap-assisted-tunneling is less sensitive to strain than BAT. In the most extreme case for TAT, we find that the current increases by about 20 times with a compressive stress of 2 GPa.

In summary, we provided a first step to understand the effects of strain on the leakage current of trap and BAT-dominated p–n junctions. Our parameter-free band-to-band model reproduces the current–voltage characteristics of our measurements but overestimates the response to strain. We believe that high doping affects the bandgap response to strain. To settle this question, measurements at higher strains, different strain configurations, and a more comprehensive model are required.

We also determined that trap energies and lifetimes are affected by strain. However, the nature of this dependence is not yet clear. This question should be addressed by an atomistic study of the response to strain of known trap states, similar to recent work on interstitials[6] and trap states in semiconductors.[5]

Finally, the tunneling processes studied in this work are the same driving the current in TFET devices. The results of this work regarding the interplay of strain, voltage, doping, and the transition from TAT to band-to-band-assisted tunneling should be useful in the design of TFETs with improved subthreshold slopes.

Conflict of Interest

The authors declare no conflict of interest.

Author Contributions

Felipe Murphy-Armando: Data curation (lead); Formal analysis (lead); Investigation (lead); Methodology (lead); Software (lead); Validation (lead); Visualization (lead); Writing—original draft (lead); Writing—review & editing (lead). **Chang Liu**: Data curation (equal); Writing—original draft (supporting). **Yi Zhao**: Conceptualization (supporting); Supervision (equal); Writing—original draft (supporting). **Ray Duffy**: Conceptualization (equal); Writing—original draft (supporting); Writing—review & editing (supporting).

Data Availability Statement

The data that support the findings of this study are available from the corresponding author upon reasonable request.

[1] International Roadmap for Devices and Systems **2023**. https://irds.ieee.org/editions/2023.

[2] Y. Song, H. Zhou, Q. Xu, J. Luo, H. Yin, J. Yan, H. Zhong, *J. Electron. Mater.* **2011**, *40*, 1584.

[3] E. Ungersboeck, V. Sverdlov, H. Kosina, S. Selberherr, *ICSICT-2006: 2006 8th Int. Conf. on Solid-State and Integrated Circuit Technology Proc.*, Shangai, China, Oct. 23–26, **2007**, p. 124.

[4] M. A. Mircovich, J. Kouvetakis, J. Menéndez, *J. Appl. Phys.* **2024**, *135*, 124501.

[5] F. Zhao, M. E. Turiansky, A. Alkauskas, C. G. Van de Walle, *Phys. Rev. Lett.* **2023**, *131*, 056402.

[6] L. Spindlberger, J. Aberl, L. Vukušić, T. Fromherz, J.-M. Hartmann, F. Fournel, S. Prucnal, F. Murphy-Armando, M. Brehm, *Mater. Sci. Semicond. Process.* **2024**, *181*, 108616.

[7] J. Appenzeller, Y.-M. Lin, J. Knoch, P. Avouris, *Phys. Rev. Lett.* **2004**, *93*, 196805.

[8] O. M. Nayfeh, C. N. Chleirigh, J. Hennessy, L. Gomez, J. L. Hoyt, D. A. Antoniadis, *IEEE Electron Device Lett.* **2008**, *29*, 1074.

[9] R. Duffy, A. Heringa, V. C. Venezia, J. Loo, M. A. Verheijen, M. J. P. Hopstaken, K. van der Tak, M. de Potter, J. C. Hooker, P. Meunier-Beillard, R. Delhougne, *Solid State Electron.* **2010**, *54*, 243.

[10] R. Duffy, A. Heringa, J. Loo, E. Augendre, S. Severi, G. Curatola, *ECS Trans.* **2006**, *3*, 19.

[11] W. Wu, C. Liu, J. Sun, W. Yu, X. Wang, Y. Shi, Y. Zhao, *IEEE Electron Device Lett.* **2014**, *35*, 714.

[12] W. Wu, Y. Pu, J. Wang, X. Xu, J. Sun, Z. Yuan, Y. Shi, Y. Zhao, *Appl. Phys. Lett.* **2013**, *102*, 093502.

[13] A. Schenk, *Solid State Electron.* **1993**, *36*, 19.

[14] G. A. M. Hurkx, H. C. de Graaf, W. J. Kloosterman, M. P. G. Knuvers, *IEEE Trans. Electron Devices* **1992**, *39*, 2090.

[15] D. Rideau, M. Feraille, L. Ciampolini, M. Minondo, C. Tavernier, H. Jaouen, A. Ghetti, *Phys. Rev. B* **2006**, *74*, 195208.

[16] X. Gonze, *Phys. Rev. B* **1997**, *55*, 10337.

[17] X. Gonze, B. Amadon, P.-M. Anglade, J.-M. Beuken, F. Bottin, P. Boulanger, F. Bruneval, D. Caliste, R. Caracas, M. Côté, T. Deutsch, L. Genovese, P. Ghosez, M. Giantomassi, S. Goedecker, D. Hamann, P. Hermet, F. Jollet, G. Jomard, S. Leroux, M. Mancini, S. Mazevet, M. Oliveira, G. Onida, Y. Pouillon, T. Rangel, G.-M. Rignanese, D. Sangalli, R. Shaltaf, M. Torrent, M. Verstraete, G. Zerah, J. Zwanzig, *Comput. Phys. Commun.* **2009**, *180*, 2582.

[18] F. Murphy-Armando, S. Fahy, *Phys. Rev. B* **2008**, *78*, 035202.

[19] F. Murphy-Armando, S. Fahy, *Phys. Rev. B* **2012**, *86*, 079903(E).

[20] F. Murphy-Armando, S. Fahy, *J. App. Phys.* **2011**, *110*, 123706.

[21] G. A. M. Hurkx, D. B. Klaassen, M. P. G. Knuvers, *IEEE Trans. Electron Devices* **1992**, *39*, 331.

[22] M. Fischetti, S. Laux, *J. Appl. Phys* **1996**, *80*, 2234.

[23] D. Schroder, *IEEE Trans. Electron Devices* **1997**, *44*, 160.

[24] J. Noffsinger, E. Kioupakis, C. G. Van de Walle, S. G. Louie, M. L. Cohen, *Phys. Rev. Lett.* **2012**, *108*, 167402.

[25] W. G. Vandenberghe, M. Fischetti, *Appl. Phys. Lett.* **2015**, *106*, 013505.

[26] F. Murphy-Armando, C. Liu, Y. Zhao, R. Duffy, *2016 13th IEEE Int. Conf. on Solid-State and Integrated Circuit Technology (ICSICT) Proc.*, Hangzhou, China, Oct. 25–28, **2016** p. 802.